Stimulated emission double depletion nanoscopy with background correction at the single-pixel level

Amirhossein Barati Sedeh,[1] Andrei Kobitski,[1] Siqing Dai,[1] Süheyla Eroğlu-Kayikçi,[2] Karin Nienhaus,[1] Lennart Hilbert,[2,3] and G. Ulrich Nienhaus[1,2,4,5,*]

[1] *Institute of Applied Physics, Karlsruhe Institute of Technology, 76131 Karlsruhe, Germany*
[2] *Institute of Biological and Chemical Systems, Karlsruhe Institute of Technology, 76344 Eggenstein-Leopoldshafen, Germany*
[3] *Zoological Institute, Karlsruhe Institute of Technology, 76131 Karlsruhe, Germany*
[4] *Institute of Nanotechnology, Karlsruhe Institute of Technology, 76344 Eggenstein-Leopoldshafen, Germany*
[5] *Department of Physics, University of Illinois at Urbana-Champaign, Urbana, Illinois 61801, USA*
[*] *uli@uiuc.edu*

Fluorescence microscopy images are inevitably tainted by background contributions including emission from out-of-focus planes, scattered light, and detector noise. In stimulated emission depletion (STED) nanoscopy, an additional, method-specific background arises from incomplete depletion and re-excitation by the depletion beam. Various approaches have been proposed to remove the background from a STED image, some of which rely on the acquisition of a separate background image that is subtracted from the STED image with a weighting factor. Using stimulated emis-sion double depletion (STEDD) nanoscopy, we observed that the weighting factor varies locally in densely labeled samples, so that background removal with a single (global) weight-ing factor generates local image artifacts due to incorrect background subtraction. Here we present an algorithm that computes the optimal weighting factor at the single-pixel level, yielding a difference image with excellent suppres-sion of low-frequency background.

Far-field o ptical fl uorescence mi croscopy is am ong th e most powerful experimental techniques in the life sciences, allowing fixed a nd l ive b iological s pecimens t o b e i maged w ith a spatial resolution of roughly half the wavelength of the excitation light. This Abbe resolution limit [1] has been overcome by ingenious super-resolution nanoscopy techniques that exploit specific physical properties of t he fl uorescence em itters [2–6]. Among these, STED nanoscopy is a raster scanning technique typically implemented in a confocal microscope [3]. At each pixel of the image, a tightly focused, approximately Gaussian excitation beam is overlaid spatially and temporally with a high-power, red-shifted depletion beam that features zero intensity at the center of the excitation beam and de-excites fluorophores in the wings of the Gaussian via stimulated emission. Ideally, only fluorophores in the central region remain electronically excited upon exposure to the depletion beam and subsequently emit fluorescence. Consequently, the two-pulse combination generates a sharpened effective excitation spot with which super-resolved images can be acquired.

In practice, a STED image is inevitably contaminated with substantial low-frequency background due to (1) incomplete depletion and (2) re-excitation by the depletion beam. Incomplete depletion originates from an imperfect overlap between the fluorescence excitation and depletion patterns, especially in peripheral regions of the confocal volume. Increasing the STED beam power alleviates this problem but causes enhanced photodamage and background due to re-excitation via anti-Stokes Raman and other light-induced processes. To minimize re-excitation, one aims to shift the wavelength of the depletion beam to the red, away from the excitation band, while still maintaining efficient stimulated emission. This strategy has its limitations, notably for emitters with broad excitation and emission bands and small Stokes shifts, e.g., core-shell quantum dots [7]. Re-excitation is of particular concern for CW-STED, which uses pulsed fluorescence excitation with asynchronous depletion by a continuous-wave laser, and various strategies have been devised to cope with this background [8–10]. A conceptually simple approach for low-frequency background removal from an STED image is the subtraction of a second image that contains only the background [7,11,12]. However, collecting a background image that perfectly mimics the background of the STED image is in general not a straightforward task.

To address the STED background problem, we have introduced stimulated emission double depletion (STEDD) nanoscopy, a method that collects STED and background image intensities within each 25-ns period between two 40-MHz excitation pulses [13]. Because STEDD nanoscopy collects signal and background intensities for each pixel within nanoseconds, it is immune to drifts and advantageous for live imaging, unlike methods that take STED and background images in succession. Moreover, it is excellent for application with quantitative techniques such as fluorescence fluctuation spectroscopy. In STEDD, each pixel is first exposed to a Gaussian excitation pulse and a conventional depletion pulse (zero center intensity). Photons collected over the first few nanoseconds are used to form the so-called STED1 image. Subsequently, a second,

~10-fold weaker depletion pulse (with intensity peaking at the center) removes the high-frequency, super-resolved signal component, and only low-frequency background persists, and those photons are collected in the STED2 image. The delay between the two depletion pulses is adjusted with a delay line according to the fluorescence lifetime of the dye marker, making sure that most detected photons contribute to the high-frequency STED1 image. Consequently, the signal-to-noise ratio is not markedly reduced with respect to regular STED imaging. The oversampled, low-frequency STED2 image is pixel-averaged to compensate for its poorer photon statistics, and the final STEDD image is calculated by subtracting the two images pixel by pixel,

$$I_{\mathrm{STEDD}} = I_{\mathrm{STED1}} - \gamma I_{\mathrm{STED2}}, \qquad \textbf{(1)}$$

where the weighting factor γ depends on the time delay between two depletion pulses. Evidently, the quality of the background correction crucially rests on choosing the proper background weighting. Different criteria can be envisioned according to which the optimal weighting factor γ can be determined. Earlier, we presented a sophisticated procedure, based on the criterion that high-frequency components should be maximized in the spatial frequency spectrum of the optimally corrected STEDD image [14]. Alternatively, one may simply increase γ up to the point that negative pixel intensities appear, or perform a least-squares minimization,

$$\gamma = \arg\min \|I_{\mathrm{STED1}} - \gamma' I_{\mathrm{STED2}}\|_2^2, \qquad \textbf{(2)}$$

to find the best estimate of γ [15], which implicitly assumes that most pixels in the image represent background. Background removal with a single, global γ value yielded overall satisfactory STEDD images, regardless of the chosen method.

However, in images of densely labeled biological samples featuring widely varying pixel intensities, we observed local artifacts, suggesting that the factor γ depends on local image properties. Notably, subtraction of the intrinsic STED background calls for a γ parameter markedly greater than one to account for the fluorescence intensity decay. In low-intensity pixels, however, a (random) detector noise becomes prevalent, which should be subtracted using $\gamma = 1$.

In this work, we present a refined method, which determines γ locally in windows centered on each pixel and subtracts the background of the pixel accordingly. For each window, we identify the best local estimate of γ, which is done here for simplicity according to Eq. (2). Our method is simple yet powerful and is applicable to other imaging modalities involving the subtraction of background images. However, there is an important caveat: the method requires that the frequency spectra of the signal and the background should not overlap appreciably, which is usually fulfilled in super-resolution microscopy.

We carefully evaluated our algorithm with STEDD images of cell nuclei of zebrafish embryos after fixation at the sphere stage [16,17]. They were immunolabeled with the dye STAR RED (Abberior) using antibodies against the RNA polymerase II (Pol II) protein. Thus, fluorescence from images of cell nuclei displays the distribution of Pol II, which is known to form clusters near transcription-active genes.

STEDD images were taken on our custom-built microscope (Fig. 1). Fluorescence was excited with a 100-ps pulsed diode laser (640 nm, 3.20 µW, 40 MHz, LDH-P-C-640B, PicoQuant). For fluorescence depletion, light pulses from a femtosecond titanium:sapphire laser (779 nm, 66 mW, 40 MHz, Mai Tai HP,

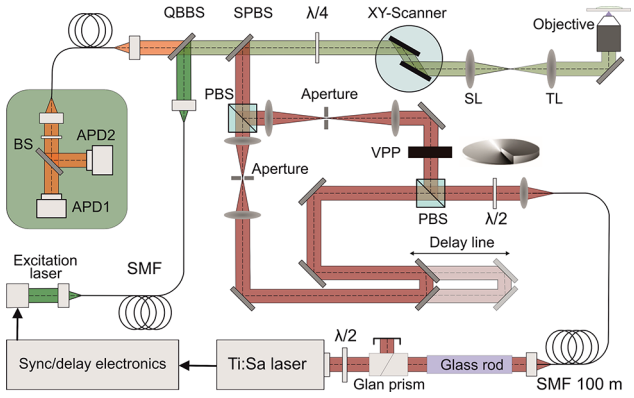

Fig. 1. Simplified schematic of the STEDD microscope. APD, avalanche photodiode; BS, non-polarizing beam splitter; PBS, polarization-maintaining beam splitter; QBBS, quad-band beam splitter; SL, scan lens; SMF, single mode fiber; SPBS, 700-nm short pass beam splitter; TL, tube lens; VPP, vortex phase plate; $\lambda/4$, quarter-wave plate; $\lambda/2$, half-wave plate. For details, see the text.

Newport Spectra-Physics) were stretched to 300 ps, and split with a polarization-maintaining beam splitter to deliver 90% of the power to the vortex phase-modulated STED1 pulse and 10% to the delayed Gaussian STED2 pulse. The delay between the excitation and STED1 pulse peaks was 200 ps; the delay between STED1 and STED2 pulses was set to 4.5 ns with a delay line (Fig. 1). Images were acquired from a $15 \times 15\ \mu m^2$ area with 5× line repetition, a pixel dwell time of 20 µs, and a step size of 30 nm. Photons were detected with avalanche photodiodes, and time-correlated single-photon counting (TCSPC) allowed us to generate separate images from photons collected before (I_{STED1}) and after (I_{STED2}) the STED2 pulse.

For noise suppression, the STED1 image was filtered with a low-pass Gaussian filter with a standard deviation $\sigma = 0.5$ pixels, corresponding to a full width at half maximum (FWHM) of 35 nm, which is roughly half of the width of the point spread function (PSF) for STED resolution and thus does not spoil the super-resolution features of the image. The oversampled, low-frequency STED2 image was filtered with a low-pass Gaussian filter with a standard deviation $\sigma = 2$ pixels, corresponding to a FWHM of 141 nm. Importantly, this is markedly less than the width of the lateral PSF for confocal imaging, which was determined as 322 ± 21 nm (FWHM) using immobilized fluorescent nanobeads (Ø 40 nm, FluoSpheres, dark red fluorescent (660/680 nm), ThermoFisher Scientific) and thus does not significantly flatten the background.

Figure 2 compares globally and locally weighted background subtraction in STEDD nanoscopy. In the regular STED (STED1) image (500 × 500 pixels), distinct fluorescence from Pol II clusters in the nucleus rides on top of a strong background. By using either a global (upper right) or local (lower left, calculated in windows of 17 × 17 pixels) weighting factor γ, the background (STED2) image is subtracted from the STED1 image to yield the STEDD image, showing significant differences between the two approaches. Background removal with locally determined γ parameters leads to an even distribution of the fluorescence of Pol II clusters, whereas the treatment with $\gamma = 7.9$ for the entire image leaves excess background at the edges of the cell nucleus, and extended blank areas appear at the center, suggesting that too much background was subtracted.

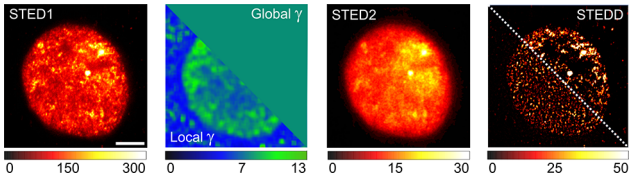

Fig. 2. Background correction of STED images according to Eq. (1) using local and global weighting parameters γ. A super-resolution (STED1) image of a cell nucleus of a zebrafish embryo (scale bar, 3 µm) is processed by subtracting, with globally (upper right) and locally (lower left) determined maps of the weighting factor γ, a background (STED2) image to yield the corresponding STEDD difference image.

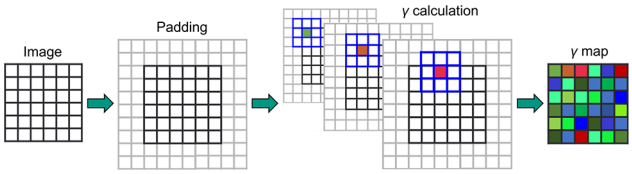

Fig. 3. Schematic depiction of the algorithm for local calculation of the background weighting factor γ. The input images (here STED1 and STED2, black pixels) are padded around the edges (gray pixels). For a small square region (blue), the weighting parameter γ is computed with Eq. (2) and assigned to the central pixel. The process is repeated for each pixel, and the data are compiled in a γ map.

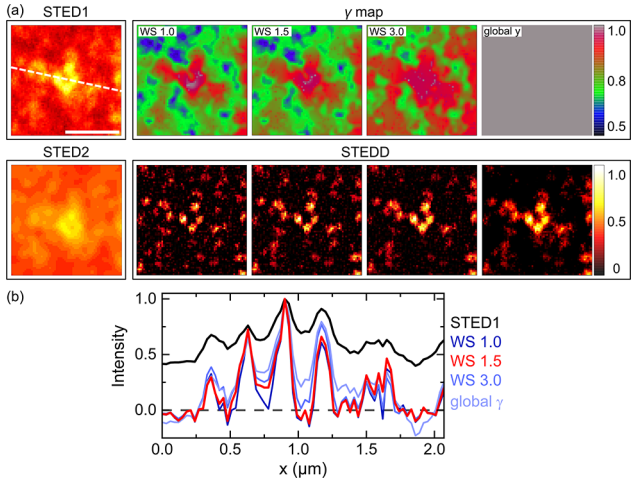

Fig. 4. Dependence of the STEDD image on the size of the background calculation window. (a) Left: High-resolution (STED1) and background (STED2) close-ups of a cell nucleus of a zebrafish embryo (scale bar, 1 µm), the color scale as in Fig. 1. Right: (top) γ maps and (bottom) resulting STEDD difference images, calculated for different window sizes (WS) and global correction. These images have been intensity-normalized in the range [0,1] to reveal changes in the shapes of the features. (b) Normalized STEDD intensity profiles along the dashed line in the STED1 image [panel (a)], generated with global and local corrections with different window sizes. Also shown is the profile of the raw STED1 image.

The algorithm for local computation of the γ parameter is shown schematically in Fig. 3. The STED1 and STED2 images are first padded around the edges to allow for identical window sizes, using a symmetric replication of the edge pixel intensities. The γ parameter is calculated for square windows (with odd pixel numbers) by using Eq. (2) and assigned to the central pixel. Pixel-by-pixel, we thus obtain a complete γ map for the entire image. The local windows should be large enough to capture slow variations of the background, so that the optimization with Eq. (2) is meaningful. A lower bound on the window size is given by the confocal PSF at the excitation wavelength, which describes spatial variations of the STED background due to incomplete depletion. The re-excitation background generates broader features due to the longer wavelength and the less focused spot of the depletion beam (donut or bottle). Image blurring from out-of-focus fluorescence also generates broader features. Taken together, a window size somewhat above the width of the confocal PSF appears suitable.

To assess the impact of the local window size for γ determination on the quality of the STEDD images, we inspected the changes of local features in the images as the window size was varied. As an example, STED1 and STED2 close-up images (67×67 pixels) are displayed in Fig. 4(a). Comparison of the γ maps and the associated STEDD images for window sizes of 11×11, 17×17, and 33×33 pixels (denoted WS 1.0, WS 1.5, and WS 3.0, respectively, with a pixel number scaled to the FWHM of the confocal PSF) shows that the γ maps become blurrier with increasing WS. Concomitantly, low-intensity (black) regions become more extended in the STEDD images because the excess background is subtracted from low-intensity pixels that are surrounded by high-intensity pixels in the local window. As a remedy to this overshoot, we also calculate γ for each pixel within a tiny window (3×3 pixels) and take this value for pixels having negligible signal intensity, defined by $I_{\mathrm{STED1}} \le \gamma(I_{\mathrm{STED2}} + \delta)$, with δ being the standard deviation of I_{STED2} in the window. Negative pixel intensities are set to zero in the final step. In line profiles (Fig. 4(b)), peaks become broader and less separated with increasing WS, suggesting that a local background correction with WS 1.0–1.5 is most effective for background removal.

The full-scale image of a cell nucleus in Fig. 5 provides another comparison of globally and locally weighted background subtraction. In the STEDD image, a global weighting factor yields high intensities in the peripheral and extended zero-intensity regions due to excess subtraction in the center, whereas local background weighting generates evenly dispersed clusters of Pol II enzymes (Fig. 5(a)), as is clearly seen in the close-ups. The line profile through the close-up view in Fig. 5(b) shows that the high-resolution features ride on a huge background pedestal in the raw STED1 image. The correction with a global γ parameter causes extended regions of negative intensity (overshoot) to appear, which must be set to zero and is avoided when using local γ values. The corresponding line profile proves that even weak features in the raw image are faithfully reproduced.

In conclusion, we have presented a method for local determination of the weighting factor γ for the subtraction of signal and background images in STEDD nanoscopy. For each pixel, the optimal γ value is obtained from an analysis within a local window. Importantly, the size of the window should be somewhat above the FWHM of the confocal PSF to yield a balanced background correction in regions of low and high intensities and varying background levels. Here, we have used computationally efficient least-squares fitting [15] to extract the optimal γ, but other algorithms [14] could be used as well. The resulting super-resolution STEDD images feature a low residual background

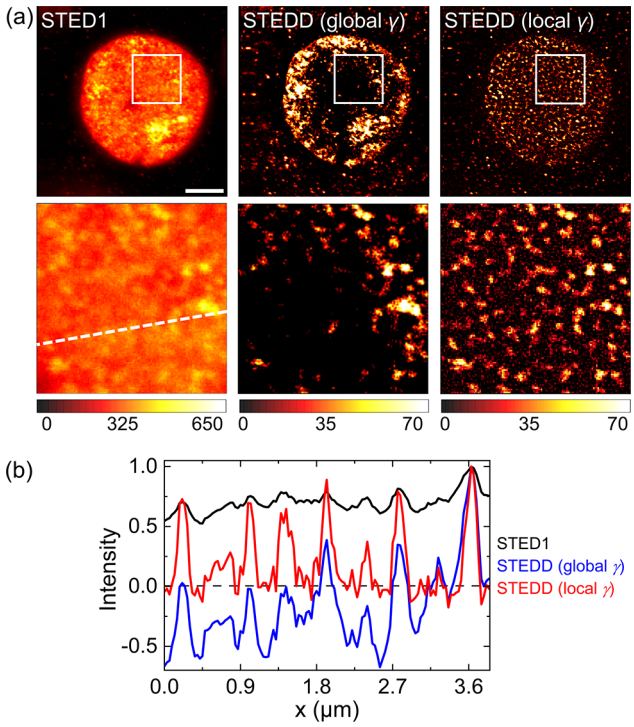

Fig. 5. Comparison of a raw STED1 image with the corresponding STEDD images of a cell nucleus of a zebrafish embryo, background-corrected with a global and a local weighting factor γ. (a) Top left, raw STED1 image (scale bar, 3 μm); middle, STEDD image (global γ), right: STEDD image (local γ, WS 1.5). Bottom: close-ups of the regions marked by the white squares in the top row. (b) Normalized intensity profiles along the dashed line in panel (a) (bottom).

and minimal subtraction artifacts, on which detailed nanoscale analyses of the morphology of Pol II clusters [16,17] and other biological structures can be based.

Finally, we note that our local background subtraction approach should be applicable to other scanning microscopy variants that rely on image subtraction, including alternative STED approaches [7,11,18], as well as microscopy techniques such as the switching laser mode (SLAM) [19], fluorescence emission difference (FED) [20], and differential-aberration two-photon excited fluorescence (DA-TPEF) microscopy [21].

Funding. Helmholtz Association (Materials Systems Engineering; Natural, Artificial and Cognitive Information Processing); Deutsche Forschungsgemeinschaft (GRK 2039); Karlsruhe School of Optics and Photonics (KSOP).

Disclosures. The authors declare no conflicts of interest.

Data availability. Data underlying the results presented in this paper are not publicly available at present but may be obtained from the authors upon reasonable request.

REFERENCES

1. E. Abbe, Archiv f. mikrosk. Anatomie **9**, 413 (1873).
2. E. Betzig, G. H. Patterson, R. Sougrat, O. W. Lindwasser, S. Olenych, J. S. Bonifacino, M. W. Davidson, J. Lippincott-Schwartz, and H. F. Hess, Science **313**, 1642 (2006).
3. S. W. Hell, Science **316**, 1153 (2007).
4. C. Werner, M. Sauer, and C. Geis, Chem. Rev. **121**, 11971 (2021).
5. K. Nienhaus and G. U. Nienhaus, J. Mol. Biol. **428**, 308 (2016).
6. M. Lelek, M. T. Gyparaki, G. Beliu, F. Schueder, J. Griffié, S. Manley, R. Jungmann, M. Sauer, M. Lakadamyali, and C. Zimmer, Nat. Rev. Methods Primers **1**, 39 (2021).
7. J. Hanne, H. J. Falk, F. Görlitz, P. Hoyer, J. Engelhardt, S. J. Sahl, and S. W. Hell, Nat. Commun. **6**, 7127 (2015).
8. Y. Ma and T. Ha, Phys. Biol. **16**, 051002 (2019).
9. G. Vicidomini, G. Moneron, K. Y. Han, V. Westphal, H. Ta, M. Reuss, J. Engelhardt, C. Eggeling, and S. W. Hell, Nat. Methods **8**, 571 (2011).
10. L. Lanzanò, I. Coto Hernández, M. Castello, E. Gratton, A. Diaspro, and G. Vicidomini, Nat. Commun. **6**, 6701 (2015).
11. G. Vicidomini, G. Moneron, C. Eggeling, E. Rittweger, and S. W. Hell, Opt. Express **20**, 5225 (2012).
12. J.-C. Lee, Y. Ma, K. Y. Han, and T. Ha, ACS Photonics **6**, 1789 (2019).
13. P. Gao, B. Prunsche, L. Zhou, K. Nienhaus, and G. U. Nienhaus, Nat. Photonics **11**, 163 (2017).
14. P. Gao and G. U. Nienhaus, Opt. Lett. **42**, 831 (2017).
15. S. Tu, X. Liu, D. Yuan, W. Tao, Y. Han, Y. Shi, Y. Li, C. Kuang, X. Liu, and Y. Yao, ACS Photonics **9**, 3863 (2022).
16. A. Pancholi, T. Klingberg, W. Zhang, R. Prizak, I. Mamontova, A. Noa, M. Sobucki, A. Y. Kobitski, G. U. Nienhaus, V. Zaburdaev, and L. Hilbert, Mol. Syst. Biol. **17**, e10272 (2021).
17. W. Zhang, A. Noa, K. Nienhaus, L. Hilbert, and G. U. Nienhaus, J. Phys. D: Appl. Phys. **52**, 414001 (2019).
18. L. Kastrup, H. Blom, C. Eggeling, and S. W. Hell, Phys. Rev. Lett. **94**, 178104 (2005).
19. H. Dehez, M. Piché, and Y. De Koninck, Opt. Express **21**, 15912 (2013).
20. S. You, C. Kuang, Z. Rong, and X. Liu, Opt. Express **22**, 26375 (2014).
21. A. Leray, K. Lillis, and J. Mertz, Biophys. J. **94**, 1449 (2008).